ChemComm

Accepted Manuscript

This article can be cited before page numbers have been issued, to do this please use: Y. Li, C. Yang and X. Yan, *Chem. Commun.*, 2017, DOI: 10.1039/C6CC10188G.

This is an Accepted Manuscript, which has been through the Royal Society of Chemistry peer review process and has been accepted for publication.

Accepted Manuscripts are published online shortly after acceptance, before technical editing, formatting and proof reading. Using this free service, authors can make their results available to the community, in citable form, before we publish the edited article. We will replace this Accepted Manuscript with the edited and formatted Advance Article as soon as it is available.

You can find more information about Accepted Manuscripts in the author guidelines.

Please note that technical editing may introduce minor changes to the text and/or graphics, which may alter content. The journal's standard Terms & Conditions and the ethical guidelines, outlined in our author and reviewer resource centre, still apply. In no event shall the Royal Society of Chemistry be held responsible for any errors or omissions in this Accepted Manuscript or any consequences arising from the use of any information it contains.

ROYAL SOCIETY OF CHEMISTRY

rsc.li/chemcomm

ChemComm

View Article Online
DOI: 10.1039/C6CC10188G

COMMUNICATION

Controllable preparation of core-shell magnetic covalent-organic framework nanospheres for efficient adsorption and removal of bisphenols in aqueous solution

Received 00th January 20xx,
Accepted 00th January 20xx

DOI: 10.1039/x0xx00000x

www.rsc.org/

Yang Li,[a] Cheng-Xiong Yang,*[a] and Xiu-Ping Yan*[ab]

We herein report a monomer-mediated in situ grow strategy for controllable construction of porous nanospheres with a magnetic core and tunable COF shell. The composite exhibits high stability and excellent performance for removal of a typical class of endocrine-disrupting chemicals, bisphenol chemicals in aqueous solution.

Covalent organic frameworks (COFs) are an emerging class of crystalline porous polymers with atomically precise design, highly ordered organic building blocks and discrete pores.[1-5] The unique features of periodic and porous structures, large surface area, low density and abundant functional groups on the channel walls make COFs excellent candidates for a variety of applications in gas adsorption,[6] separation,[7,8] catalysis,[9] optoelectronic devices[10] and sensing[11]. Nevertheless, COFs are generally irregular in morphology and it is hard to control their growth rationally. As a result, shapeless bulk materials are always formed.[12,13] Besides, the light density makes COF materials difficult to precipitate from the matrix. These unexpected disadvantages bring inconvenience and obstacle in their further use as well as low efficiency in adsorption process. Therefore, controllable synthesis of COFs or their composites with uniform particle sizes is of considerable significance in promoting wide applications of COFs.

Combining the functional components to acquire core-shell-type composite materials has gained burgeoning attention in recent years, as such composites enable elegant combination of physical and chemical properties, synergistic effects and multiple functions of individual components.[14,15] Composite materials with magnetic cores are attractive for wide applications[16-20] because the remarkable superparamagnetism, stability and biocompatibility endow them with great manoeuvrability, fast separation and enhanced performance with the help of magnetic field. Moreover, the surface of magnetic nanocomposites can be grafted with a wide variety of functional moieties, making further reaction and modification convenient.

Incorporation of the merits of COFs and magnetic nanoparticles to construct a novel class of nanocomposites with both enhanced functionality and magnetic separability is of great significance and interest. In particular, the solid spherical magnetic cores can offer a center for COF growth and crystallization at all directions equally, which provides a possibility for controllable synthesis of magnetic core-shell COFs. Though a few works on the growth of COF thin film or membrane on graphene, highly oriented pyrolytic graphite (HOPG) and Al_2O_3 have been reported,[21-23] controllable growth of COFs on the surface of nanoparticles to form tunable core-shell structure materials remains a challenge to be explored.

Herein, we show a monomer-mediated in situ growth strategy for controllable growth of COF shells on magnetic nanospheres to construct magnetic core-shell COF nanospheres. As a proof of concept, super-paramagnetic Fe_3O_4 nanospheres are used as the core, while a highly stable porous COF, TpBD[24,25] (Tp and BD refer to 1,3,5-triformylphloroglucinol and benzidine, respectively) is chosen as the shell. The core Fe_3O_4 nanospheres are functionalized with a monomer Tp of the COF to facilitate the growth of a uniform shell of COF with marvelous stability. The thickness of the crystal COF shell is tailored by tuning the monomer concentration. The

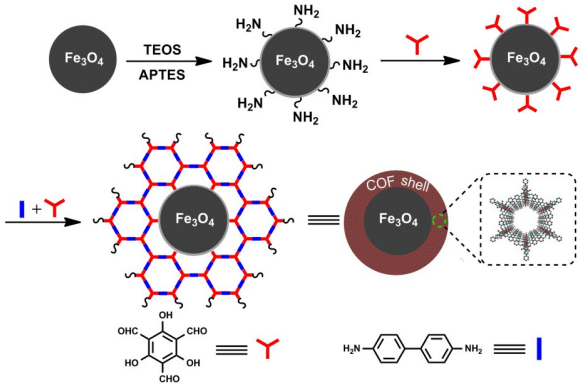

Fig. 1 Illustration for the monomer-mediated in situ growth strategy for the synthesis of core-shell Fe_3O_4@TpBD nanospheres.

[a] College of Chemistry, Research Center for Analytical Science, Tianjin Key Laboratory of Molecular Recognition and Biosensing, State Key Laboratory of Medicinal Chemical Biology, Nankai University, Tianjin 300071, China
[b] Collaborative Innovation Center of Chemical Science and Engineering (Tianjin), Tianjin 300071, China. E-mail: cxyang@nankai.edu.cn; xpyan@nankai.edu.cn

† Electronic Supplementary Information (ESI) available: Synthetic procedure and compound characterization. See DOI: 10.1039/x0xx00000x

prepared magnetic core-shell COF nanospheres show promising for fast removal of typical endocrine-disrupting chemicals (EDCs), bisphenol A (BPA) and bisphenol AF (BPAF)[26,27] from aqueous solution with high adsorption capacity and excellent reusability. The proposed approach offers a platform for rational design of magnetic core-shell COF architectures as promising adsorbents to remove toxic pollutants.

Fig. 1 shows our monomer-mediated in situ growth strategy for the synthesis of the core-shell Fe_3O_4@TpBD nanospheres. Briefly, the Fe_3O_4 nanospheres were prepared according to the literature protocol with some modifications (ESI†).[28] Tetraethyl orthosilicate (TEOS) and (3-aminopropyl)triethoxysilane (APTES) were added to protect the magnetic core from aggregation and to introduce -NH_2 on the surface of Fe_3O_4 to form amino functionalized nanospheres (Fe_3O_4-NH_2). Then, Tp, a monomer of TpBD, was grafted onto the surface of the Fe_3O_4-NH_2 via Schiff base reaction for subsequent in situ growth of the COF shell. Thus, core-shell Fe_3O_4@TpBD nanospheres were prepared (See ESI† for details).

Pre-grafting of a monomer of TpBD on the surface of Fe_3O_4 is of crucial importance to acquire uniform crystalline COF shells. In a preliminary effort, we tried to directly grow TpBD on Fe_3O_4 without silanization reagent nor Tp coating, but we observed the aggregation of Fe_3O_4 and the self-assembly of uncontrollable bulk TpBD rather than TpBD shells on the surface of Fe_3O_4 (Fig. S1a,b, ESI†). We then made a further effort to grow TpBD on Fe_3O_4-NH_2, but the COF still failed to grow around the core uniformly to constitute the shell though the dispersibility of Fe_3O_4 core was improved (Fig. S1c,d, ESI†). We also tried a layer-by-layer method to grow TpBD shell on Fe_3O_4-NH_2 (ESI†), and did observe the core-shell structure and the increase of the shell thickness as the grow cycles increased (Fig. S2a-c, ESI†). However, we obtained amorphous structure instead of crystal COF shells due to the broad peaks between 20° to 30° and no peaks below 10° in X-ray diffraction (XRD) pattern (Fig. S2d, ESI†). To achieve the growth of uniform crystalline COF shells, we developed a monomer-mediated in situ growth strategy for controllable growth of COF shells with the use of Tp pre-grafted Fe_3O_4 as the starting material. The pre-grafted Tp acts as a bridge between the core and shell to acquire better interaction, and offers nucleate center for COF growth to improve the uniformity of the shell structure (Fig. 1).

The type of solvent, the concentration of monomers and the reaction time are also key factors to control the crystallinity and thickness of TpBD shells. Partial monomer dissolution in solvent was reported to control the diffusion of the monomers into solution and promote the nucleation process.[29,30] We screened a variety of solvent combinations, for instance, ethanol/toluene, ethanol/dioxane, toluene/dioxane and mesitylene/dioxane,. We found the combination of mesitylene/dioxane provided the highest XRD intensity (Fig. S3, ESI†). Increase of the reaction time greatly improved the crystallinity of the TpBD shells with little increase in thickness (Fig. S4 and S5, ESI†), indicating that a time-dependent self-correction process may occur in the COF shells to assist in the formation of an ordered crystalline structure.[1,4] The thickness of the COF shell (from 15 nm to 65 nm) in TEM images and the peak intensity of TpBD at 3.3° in XRD pattern increased with the concentration of COF monomers (Fig. S6, ESI†). The above results show that control of solvent, the concentration of monomers and

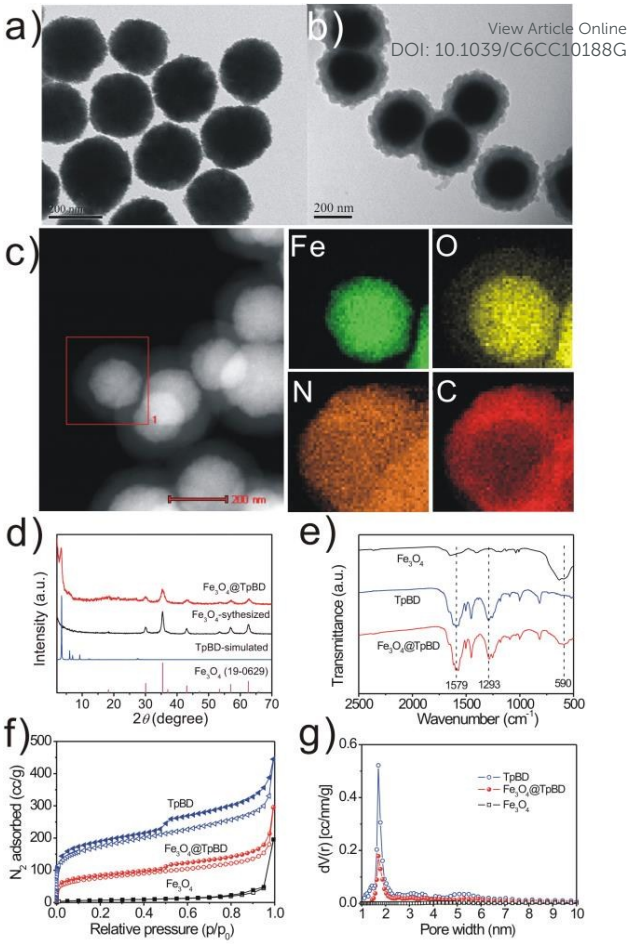

Fig. 2 (a) TEM images of Fe_3O_4. (b) TEM images of Fe_3O_4@TpBD. (c) HAADF-STEM image and EDX elemental mapping of Fe_3O_4@TpBD. (d) XRD patterns of TpBD, Fe_3O_4 and Fe_3O_4@TpBD. (e) FT-IR spectra of TpBD, Fe_3O_4 and Fe_3O_4@TpBD. (f) Nitrogen adsorption-desorption isotherms of TpBD, Fe_3O_4 and Fe_3O_4@TpBD. (g) Pore size distribution of Fe_3O_4, TpBD and Fe_3O_4@TpBD.

the reaction time enables a tunable growth of crystal TpBD shells in the composite.

The peaks for Si–O vibration at 1080 $cm^{-1}$and for the C=O stretching at 1629 cm^{-1} in Fourier transform-infrared (FT-IR) spectra show the successful silanization coating and Tp functionalization on Fe_3O_4, respectively (Fig. S7, ESI†). The Zeta potential of Fe_3O_4 changed from -29 mV to -11 mV and -15 mV after decorating the amino groups and TpBD shells, respectively (Table S1, ESI†). The introduction of TpBD shells onto Fe_3O_4 led to an obvious size increase (Table S1 and Fig. S8, ESI†).

Transmission electron microscope (TEM), high angle annular dark field scanning transmission electron microscopy (HAADF-STEM) and energy-dispersive X-ray spectroscopy (EDX) elemental mapping data reveal a typical core-shell structure of such obtained product Fe_3O_4@TpBD nanospheres (Fig. 2a-c). XRD pattern shows the Fe_3O_4@TpBD has characteristic peaks for the face center cubic (fcc) structure of Fe_3O_4 in a range of 20°-70° (JCPDS no. 19-0629) as well as those at low angles of 3.3° and 6.0° for the (100) and (200) reflection planes of simulated TpBD in eclipsed packing manner TpBD (Fig. 2d).[24] FT-IR spectra exhibit Fe-O stretching band at 590 cm^{-1} of Fe_3O_4 and the characteristic peaks of TpBD, such as aromatic C=C stretching at 1453 cm^{-1} and 1579 cm^{-1} and C–N stretching vibration at 1293 cm^{-1} (Fig. 2e). The results also verify the keto form

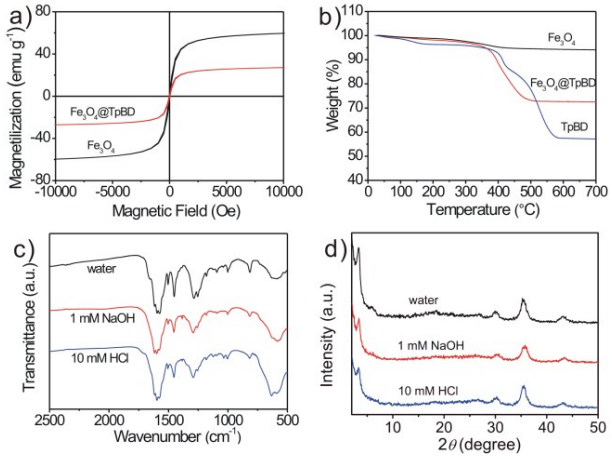

Fig. 3 (a) Magnetic hysteresis loops of Fe_3O_4 and Fe_3O_4@TpBD. (b) TGA curves of Fe_3O_4, TpBD and Fe_3O_4@TpBD. (c) FT-IR spectra and (d) XRD pattern of Fe_3O_4@TpBD treated with HCl, NaOH and water for 3 days.

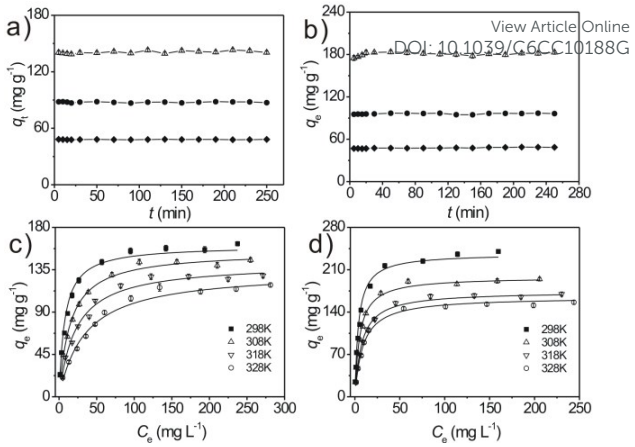

Fig. 4 (a) Time-dependent adsorption of BPA. (b) Time-dependent adsorption of BPAF on Fe_3O_4@TpBD. (c) Adsorption isotherms of BPA on Fe_3O_4@TpBD. (d) Adsorption isotherms of BPAF on Fe_3O_4@TpBD. The solid lines were obtained by the Langmuir model simulation.

of TpBD in the composite.[25] The prepared Fe_3O_4@TpBD gave a typical TpBD pore size of 1.70 nm and an enhanced BET surface area and pore volume of 272.6 $m^2 g^{-1}$ and 0.457 $cm^3 g^{-1}$ (cf. 26.98 $m^2 g^{-1}$ and 0.0545 $cm^3 g^{-1}$ for Fe_3O_4), respectively (Fig. 2f,g; Table S2, Fig. S9, ESI†). The above results demonstrate the enhanced surface area and porosity in Fe_3O_4@TpBD. Fe_3O_4@TpBD also shows superparamagnetism with M_s value of 22 emu g^{-1} due to no obvious coercivity or remanence (Fig. 3a).

The as-synthesized Fe_3O_4@TpBD nanospheres also possess good stability. Thermogravimetric analysis (TGA) shows that Fe_3O_4@TpBD has good thermal stability up to 350 ℃ (Fig. 3b). To address its chemical stability, Fe_3O_4@TpBD was immersed in water, 10 mmol L^{-1}HCl, and 1 mmol L^{-1}NaOH for 3 days, and then analyzed by XRD and FT-IR. The results show that no significant changes in the XRD pattern and FT-IR spectra of the Fe_3O_4@TpBD were observed (Fig. 3c,d). The above observations indicate that Fe_3O_4@TpBD has sufficient stability for subsequent applications.

Next we applied the porous crystal Fe_3O_4@TpBD as promising candidate for effective adsorption and removal of typical EDCs (BPA and BPAF) from aqueous solution. Fe_3O_4@TpBD with a COF thickness of 65 nm was chosen for the better adsorption capacity and faster magnetic separation (Fig. S10, ESI†). Fe_3O_4@TpBD shows fast adsorption kinetics for BPA and BPAF. The adsorption equilibrium for BPA and BPAF on Fe_3O_4@TpBD was achieved within 5 min (Fig. 4a,b). The adsorption of BPA and BPAF on Fe_3O_4@TpBD follows the pseudo-second-order kinetic model (Table S3, Fig. S11 and S12, ESI†), suggesting that the adsorption is based on the adsorption capacity of the surface sites on Fe_3O_4@TpBD at equilibrium.[31] The adsorption isotherms of BPA and BPAF on Fe_3O_4@TpBD shows a typical Langmuir adsorption with the maximum adsorption capacities of 160.6 and 236.7 mg g^{-1}, respectively (Fig. 4c,d; Table S4, ESI†), indicating a monolayer adsorption with a limited number of sites on the sorbent.[32] No obvious change of the adsorption capacity for the adsorption of BPAF and BPA at pH 7 was found when the salt concentration increased up to at least 100 mmoL L^{-1} (Fig. S13, ESI†). pH change from 3 to 10 only led to a slight decrease of the adsorption capacity due to the deprotonation of BPAF and BPA under alkaline conditions[31,33] and the electrostatic repulsion between the analytes and Fe_3O_4@TpBD (Fig. S14, ESI†). Compared to other adsorbents, Fe_3O_4@TpBD displayed higher adsorption capacities with faster adsorption kinetics for the adsorption of BPAF and BPA (Table S5).

The adsorption of BPAF and BPA on Fe_3O_4@TpBD is a thermodynamically spontaneous process with both negative enthalpy and entropy changes (Table S6, Fig. S15, ESI†). Fe_3O_4@TpBD demonstrated significant enhanced adsorption ability for BPA and BPAF compared with Fe_3O_4 (Fig. 5a,b), indicating the crucial role of the TpBD shell. π-π interaction and hydrogen bonding should be considered during the adsorption. UV-vis absorption spectra display bathochromic shift of the absorption peaks for both BPA and BPAF after their adsorption on Fe_3O_4@TpBD (Fig. S16, ESI†), indicating π-π interaction between the benzene rings of BPAF/BPA and TpBD planes. The adsorption ability of Fe_3O_4@TpBD decreased obviously for model molecules with decreased hydroxyl groups and large size (Fig. S17, ESI†), indicating the hydrogen bonding effect between the hydroxyl group in BPA and BPAF and the carbonyl groups on the channel walls in TpBD as the size of BPA and BPAF are much smaller than the channel of TpBD (Fig. 5c).[36]

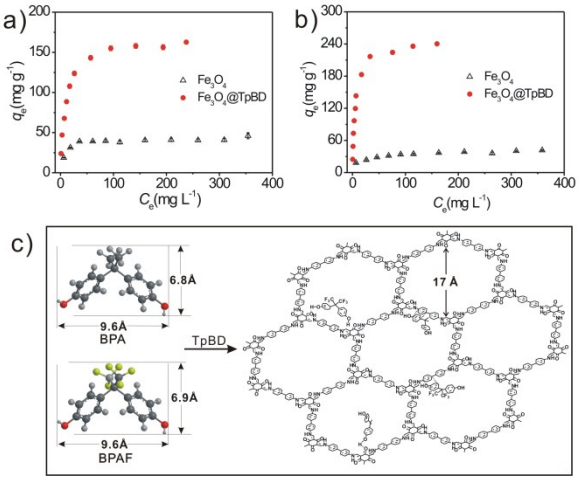

Fig. 5 Adsorption isotherms of a) BPA and b) BPAF on Fe_3O_4 and Fe_3O_4@TpBD at 298 K. c) Illustration for the mechanism of π-π interaction and hydrogen bonding between BPA/BPAF and TpBD.

The adsorbed BPA and BPAF can be easily desorbed from Fe_3O_4@TpBD with ethanol within 1 min (Fig. S18 and S19, ESI†). Fe_3O_4@TpBD also demonstrated excellent reusability for the adsorption of BPA and BPAF (Fig. S20 and S21, ESI†). These results endow Fe_3O_4@TpBD with great performance in adsorption and removal of bisphenol chemicals and immense potential as a novel type of adsorbents for aqueous solution adsorption.

In summary, we have demonstrated an efficient monomer-mediated in situ growth method to construct core-shell Fe_3O_4@COF nanospheres. The resulting composites possess porous crystalline structure, high surface area, good chemical stability and great magnetic response, thus offer great potential as promising adsorbents for rapid adsorption and removal of chemical pollutants from aqueous solution. Considering the broad diversity, unique capability and wide applications of both magnetic nanoparticles and COFs, we believe that the fabrication strategy will open up an avenue in rational design of core-shell structure with magnetic platforms and tunable porous COF shells for wide applications in various fields such as magnetic resonance imaging, targeted drug delivery and catalysis.

This work was supported by the National Basic Research Program of China (Grant 2015CB932001), National Natural Science Foundation of China (Grants 21435001, 21305071), Tianjin Natural Science Foundation (Grants 14JCZDJC37600 and 14JCQNJC06600), and the Fundamental Research Funds for the Central Universities.

Notes and references

1 X. Feng, X. S. Ding, D. L. Jiang, Chem. Soc. Rev. 2012, **41**, 6010.
2 S. Y. Ding, W. Wang, Chem. Soc. Rev. 2013, **42**, 548.
3 Z. H. Xiang, D. P. Cao, L. M. Dai, Polym. Chem.2015, **6**, 1896.
4 P. J. Waller, F. Gándara, O. M. Yaghi, Acc. Chem. Res. 2015, **48**, 3053.
5 A. P. Côté, A. I. Benin, N. W. Ockwig, M. O'Keeffe, A. J. Matzger, O. M. Yaghi, Science 2005, **310**, 1166.
6 C. J. Doonan, D. J. Tranchemontagne, T. G. Glover, J. R. Hunt, O. M. Yaghi, Nat. Chem. 2010, **2**, 235.
7 H. L. Qian, C. X. Yang, X. P. Yan, Nat. Commun. 2016, **7**, 12104.
8 C. X. Yang, C. Liu, Y. M. Cao, X. P. Yan, Chem. Commun. 2015, **51**, 12254.
9 S. Y. Ding, J. Gao, Q. Wang, Y. Zhang, W. G. Song, C. Y. Su, W. Wang, J. Am. Chem. Soc. 2011, **133**, 19816.
10 S. Wan, J. Guo, J. Kim, H. Ihee, D. L. Jiang. Angew. Chem. Int. Ed. 2009, **48**, 5439.
11 S. Y. Ding, M. Dong, Y. W. Wang, Y. T. Chen, H. Z. Wang, C. Y. Su, W. Wang, J. Am. Chem. Soc. 2016, **138**, 3031.
12 D. N. Bunck, W. R. Dichtel, Angew. Chem. Int. Ed. 2012, **51**, 1885.
13 L. A. Baldwin, J. W. Crowe, M. D. Shannon, C. P. Jaroniec, P. L. McGrier, Chem. Mater. 2015, **27**, 6169.
14 R. G. Chaudhuri, S. Paria, Chem. Rev. 2012, **112**, 2373.
15 M. B. Gawande, A. Goswami, T. Asefa, H. Z. Guo, A. V. Biradar, D. L. Peng, R. Zboril, R. S. Varma, Chem. Soc. Rev. 2015, **44**, 7540.
16 Y. Wang, H. C. Gu, Adv. Mater. 2015, **27**, 576.
17 L. Lartigue, P. Hugounenq, D. Alloyeau, S. P. Clarke, M. Lévy, J. C. Bacri, R. Bazzi, D. F. Brougham, C. Wilhelm, F. Gazeau, ACS Nano 2012, **6**, 10935.
18 L. P. Dong, S. Feng, S. S. Li, P. P. Song, J. D. Wang, Anal. Chem. 2015, **87**, 6849.
19 X. L. Zhang, H. Y. Niu, W. H. Li, Y. L. Shi, Y. Q. Cai, Chem. Commun. 2011, **47**, 4454.
20 A. Samanta, B. J. Ravoo, Angew. Chem. Int. Ed. 2014, **53**, 12946.
21 J. W. Colson, A. R. Woll, A. Mukherjee, M. P. Levendorf, E. L. Spitler, V. B. Shields, M. G. Spencer, J. W. Park, W. R. Dichtel, Science 2011, **332**, 228.
22 X. H. Liu, C. Z. Guan, S. Y. Ding, W. Wang, H. J. Yan, D. Wang, L. J. Wan, J. Am. Chem. Soc. 2013, **135**, 10470.
23 H. Lu, C. Wang, J. J. Chen, R. L. Ge, W. G. Leng, B. Dong, J. Huang, Y. N. Gao, Chem. Commun. 2015, **51**, 15562.
24 B. P. Biswal, S. Chandra, S. Kandambeth, B. Lukose, T. Heine, R. Banerjee, J. Am. Chem. Soc. 2013, **135**, 5328.
25 S. Chandra, S. Kandambeth, B. P. Biswal, B. Lukose, S. M. Kunjir, M. Chaudhary, R. Babarao, T. Heine, R. Banerjee, J. Am. Chem. Soc. 2013, **135**, 17853.
26 Y. Q. Huang, C. K. C. Wong, J. S. Zheng, H. Bouwman, R. Barra, B. Wahlström, L. Neretin, M.H. Wong, Environ. Int. 2012, **42**, 91.
27 S. J. Song, T. Ruan, T. Wang, R.Z. Liu, G. B. Jiang, Environ. Sci. Technol. 2012, **46**, 13136.
28 J. N. Gao, X. Z. Ran, C. M. Shi, T. M. Cheng, Y. P. Su, Nanoscale 2013, **5**, 7026.
29 J. W. Colson, J. A. Mann, C. R. DeBlase, W. R. Dichtel, J. Polym. Sci. Part A: Polym. Chem. 2015, **53**, 378.
30 B. J. Smith, W. R. Dichtel, J. Am. Chem. Soc. 2014, **136**, 8783.
31 M. M. Zhou, Y. N. Wu, J. J. Qiao, J. Zhang, Amanda McDonald, G. T. Li, F. T. Li. J. Colloid. Interface Sci. 2014, **421**, 85.
32 Y. Wang, G. Q. Ye, H. H. Chen, X. Y. Hu, Z. Niu, S. Q. Ma, J. Mater. Chem. A 2015, **3**, 15292.
33 L. Zhang, J. N. Lv, T. C. Xu, L. J. Yang, X. Q. Jiang, Q. Li, Sep. Purif. Technol. 2013, **116**, 145.
34 Z. X. Jin, X. X. Wang, Y. B. Sun, Y. J. Ai, X. K. Wang, Environ. Sci. Technol. 2015, 49, 9168.
35 Song, B. H. Wei, Z. Q. Wang, X. Zhang, Smet, M. W. Dehaen, Adv. Mater.2007, **19**, 416.
36 L. L. Zhu, Y. H. Cao, G. Q. Cao, Biosens. Bioelectron. 2014, **54**, 258.